Solidification processes in Cu-Zr-Ag amorphisable alloy system

D. Janovszky, A. Sycheva, K. Tomolya, J. Geiger, J. Solyom, A. Roosz

MTA-ME, Hungarian Academy of Sciences-University of Miskolc, Materials Science Research Group, Miskolc-Egyetemvaros, H-3515, Hungary

e-mail: fekjd@uni-miskolc.hu

Abstract: The Cu-Zr-Ag system is one of Cu-Zr based bulk metallic glasses (BMG) that has been in the center of great interest for a long time. This work summarizes results on solidification in the Cu-Zr-Ag ternary alloys and relationship between the cooling rate and their microstructure. The alloys in a wide range of compositions were characterized by X-ray diffraction (XRD), scanning electron microscopy (SEM), transmission electron microscopy (TEM) and differential scanning calorimetry (DSC) techniques. The surface of stable liquidus miscibility gap has been presented by isothermal sections in this system. The central part of liquidus projection of the ternary Cu-Zr-Ag system is determined based on the harmonization of experimental results and the calculated phase diagrams. Due to the liquid separation, amorphous/crystalline composites could be obtained with a silver content up to 50 at%. The primary solidified phases were identified in different samples cooled with a controlled cooling rate (5 K/min), in the arc melting furnace (master alloys) and in a wedge shape mould. It has been shown that the m-phase (or $AgCu_4Zr$) has the lowest and the $(CuAg)_{10}Zr_7$ the highest driving force for nucleation in this system. It has been shown that the glass forming ability depends not only on the properties of atomic constituent but on the phases formed during the solidification of undercooled liquid.

Keywords: Ag-Cu-Zr alloys, Ternary alloy system, Liquid-liquid separation, Solidification, DSC

1. Introduction

Copper-zirconium based bulk metallic glasses (BMGs) have attracted much interest since the discovery of metallic glasses because of their potential advantages as engineering materials, including high tensile strength [1-5]. The ternary Cu-Zr-Ag [6-11] and Cu-Zr-Al [12-16] and quaternary Cu-Zr-Ag-Al [17-21] systems have been recently studied regarding the bulk glass forming ability (BGFA); however, only a few studies have been focused on crystallization products that may occur during solidification in the Cu-Zr-Ag alloy system. There has been no standard definition of glass forming ability (GFA) up to date; generally, this parameter is derived from the properties of atomic components or those of the produced amorphous sample.

There is a discrepancy in opinions related to the ternary eutectic composition and liquidus projection in this system. A.A. Kündig et al. [6], X.C. He et al. [7] and D.H. Kang et al. [8] published a description for this ternary alloy system. Moreover, an interesting phenomenon in the Cu-Ag system is the presence of a miscibility gap revealed by Frederiksson et al. in the liquid and solid solution [20]. Kündig et al. opine that the metastable liquid phase miscibility gap of Cu-Ag enlarges owing to the addition of Zr. He et al. did not consider the miscibility gap of the liquid phase in their calculations. The ternary liquid miscibility gap was predicted from model parameters in D.H. Kang et al.'s calculation.

In this alloy system, there is an intermetallic compound: m-phase of body-centered tetragonal structure denoted as $Cu_{70}Zr_{16}Ag_{14}$ (or $AgCu_4Zr$) by Zhou et al. [23]. The crystal

lattice of m-phase (together with the atomic positions) is not well-known in literature. Phases solidified in this alloy system were studied by diffusion triple technique [24].

The aim of the present work is the investigation of the effect of cooling rate on the microstructure, solidification products of the Cu-Zr-Ag glass forming alloy and the relationship between the solidification and the GFA of this alloy system.

2. Experimental

The master alloy ingots of Cu-Zr-Ag alloys were prepared within a wide range of compositions (Table 1). The ingots were prepared by arc melting a mixture of pure metals under argon atmosphere (min. 99.99 % v/v) with a Ti-getter. The surface of the samples being in contact with the Ar atmosphere during arc melting cooled with a minimum rate of 100 K/s. The cooling rate of the bottom surface of the samples being in contact with the inner surface of the copper crucible was considerably higher. The ingots were re-melted at least four times in order to ensure their chemical homogeneity. Typically, 15 g ingots were prepared. The ingots were re-melted in a glassy carbon crucible by induction melting, followed by centrifugal casting into wedge-shaped copper moulds under argon atmosphere. Wedge-shaped samples (with a size of 30 mm X 3 mm X 20 mm) were selected in order to analyze the influence of the cooling rate. The minimum thickness of the wedge was about 20 μm, the maximum thickness was 3 mm. According to our previous research [25], the cooling rate was above 20000 K/s near the tip of the wedge sample. At its base the cooling rate was about 2000 K/sec. The cross section of each sample was etched using 0.5% HF. The samples were examined by an 1830I Amray, Zeiss EVO MA and by a Hitachi S-4800 (for higher resolution images) scanning electron microscopes (SEM) equipped with an EDX energy dispersive X-ray spectrometer. Backscattered electron micrographs were recorded in order to get information about the composition of the phases. The thermal analysis was performed by a Netzsch 404 differential scanning calorimeter (DSC) under Ar atmosphere with heating rates from 1 to 10 K/min. Alumina crucibles were used for the measurements. One of the compositions ($Cu_{45}Zr_{36}Ag_{19}$) was heated to 1150 K (above the melting temperature) and held at this temperature for 5 minutes. After holding time was over the samples were cooled at 4 K/min and quenched at different temperatures for the detailed examination of solidification processes. The temperature was measured by a thermocouple. Transmission electron microscopic study was performed on a FEI Tecnai G2 transmission electron microscope equipped with EDX energy dispersive X-ray spectrometer. The relative error of these EDX measurements is max 5 at%. The acceleration voltage was 200 kV. The TEM sample was prepared from the thinnest edge of the wedge-like sample and thinned by ion polishing method (Gatan PIPS). Then the samples were characterized by tilt series of electron diffraction (ED) patterns, bright field images and EDX spectra.

Description and interpretation of the liquid-liquid miscibility gap were made by the Cadkey (KeyCreator) CAD design and modelling system. The wireframe and surface model were realized by fitting spline curves (parabolas) via the measured points.

3. Results and discussion

Cu-Zr-Ag is a very complicated system: it features 9 peritectic and 3 eutectic reactions according to [7-8]. The cooling rate has a significant influence on phase formation, especially in the case of amorphous alloys. Multi-component metallic alloys may become amorphous when the liquid is undercooled down to the glass transition temperature, by-passing the formation of crystalline phases.

3.1 Surface of the stable liquid miscibility gap

In our previous research [26-27], we confirmed the existence of miscibility gap in the Cu-Zr-Ag system [8, 28] and revealed its boundaries. Based on these data, the surface that delimits to the liquid separation is determined (Fig. 1). For this purpose we used the compositions of the master alloys, the related end points of tie-lines and the corresponding temperatures. The isothermal sections are shown in Fig. 1. The solidus surfaces of primary

solidification phases intersect the surface of liquid separation and continue until they reach the surface of monotectic reaction at 1174 K [26].

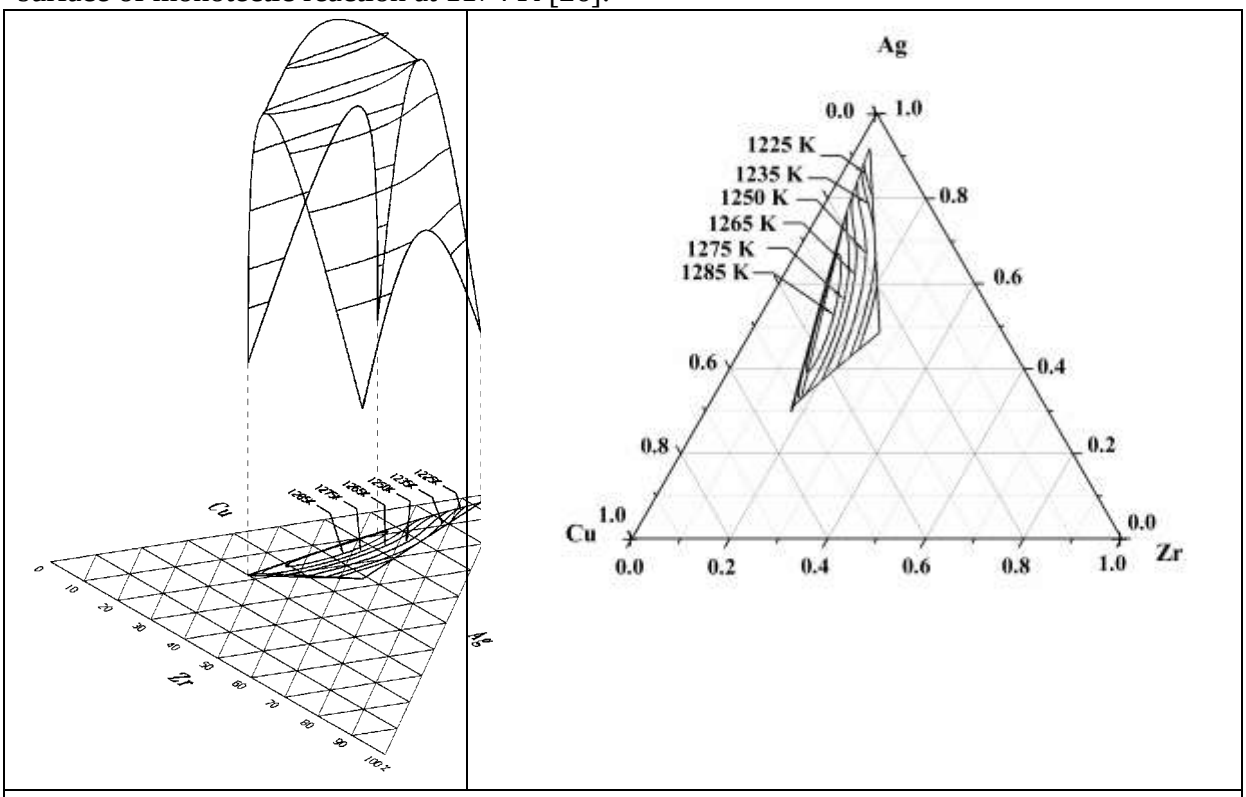

Fig. 1: Surface of the stable miscibility gap [26]: 2D and 3D view

3.2 Microstructure of samples solidified under controlled cooling rate (5 K/min (0.083 K/s))

Controlled solidification at 5 K/min (0.083 K/s) was performed in the DSC equipment in order to favor the formation of the equilibrium phases as a consequence of the low cooling rate. As a first step, three ternary eutectic compositions ($Cu_{45}Zr_{36}Ag_{19}$, $Cu_{39.7}1Zr_{41.99}Ag_{18.3}$ and $Cu_{35}Zr_{41.2}Ag_{23.8}$) published in literature were analyzed to determine the real eutectic composition. Although the three compositions are close to each other, their solidified microstructures are different. The same four phases were clearly identified in these compositions: AgZr, m-phase ($AgCu_4Zr$), $CuZr_2$ and $(CuAg)_{10}Zr_7$. According to EDX measurements, Cu is able to substitute Ag in the AgZr phase to a certain concentration of 10-18 at% since Ag and Cu have the same lattice (f.c.c.) and comparable atomic radii.

The (AgCu)Zr phase is orthorhombic (a_0=0.480 nm, b_0=0.474 nm, c_0=0.740 nm) with a measured composition of $Ag_{29}Cu_{18}Zr_{53}$. The m-phase shows a miscibility range, and its composition changes from $Cu_{58}Zr_{28}Ag_{14}$ to $Cu_{63}Zr_{22}Ag_{15}$ as reported in [24] as well. The $(CuAg)_{10}Zr_7$ phase has orthorhombic unit cell (a_0=0.940 nm, b_0=0.950 nm, c_0=1.290 nm) based on tilt series of ED patterns with a measured composition of $Cu_{42}Zr_{44}Ag_{14}$. The presence of a remarkable amount of Ag, which has a greater atomic radius than Cu, leads to an expansion of the unit cell of this phase with respect to $Cu_{10}Zr_7$ (ICSD #164881: a_0=0.935 nm, b_0=0.931 nm, c_0=1.268 nm).

The (AgCu)Zr phase is orthorhombic (a_0=0.480 nm, b_0=0.474 nm, c_0=0.740 nm) with a measured composition of $Ag_{29}Cu_{18}Zr_{53}$. The m-phase shows a miscibility range, and its composition changes from $Cu_{58}Zr_{28}Ag_{14}$ to $Cu_{63}Zr_{22}Ag_{15}$ as reported in [24] as well. The $(CuAg)_{10}Zr_7$ phase has orthorhombic unit cell (a_0=0.940 nm, b_0=0.950 nm, c_0=1.290 nm) based on tilt series of ED patterns with a measured composition of $Cu_{42}Zr_{44}Ag_{14}$. The presence of a remarkable amount of Ag, which has a greater atomic radius than Cu, leads to

an expansion of the unit cell of this phase with respect to $Cu_{10}Zr_7$ (ICSD #164881: a_0=0.935 nm, b_0=0.931 nm, c_0=1.268 nm).

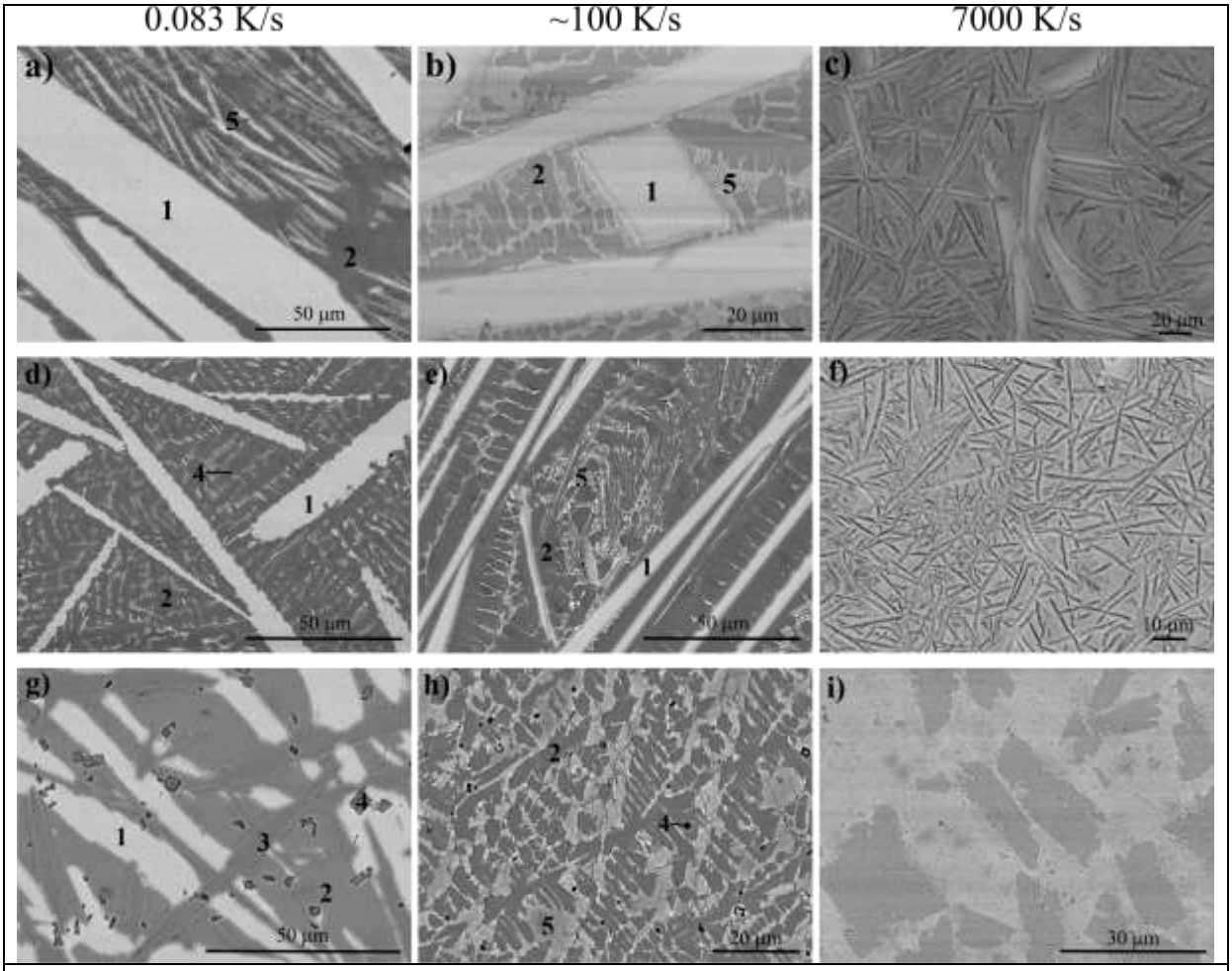

Fig. 2: Microstructure evolution of $Cu_{35}Zr_{41.2}Ag_{23.8}$ (a,b,c), $Cu_{39.71}Zr_{41.99}Ag_{18.}$(d,e,f) and $Cu_{45}Zr_{36}Ag_{19}$ (g,h,i) alloy solidified with increasing cooling rate:0.083 K/s (a, d, g), master alloy (~100 K/s) (b, e, h), wedge-shaped sample at a place with ~7000 K/s cooling rate (c, f, i): 1 – AgZr, 2 – $(CuAg)_{10}Zr_7$, 3 – m-phase, 4 – $CuZr_2$, 5 – eutectic structure

It was observed that the $Cu_{35}Zr_{41.2}Ag_{23.8}$ alloy (Fig. 2 a) does not correspond to the ternary eutectic composition, in disagreement with the results of the calculation of He et al. [7]. According to the DSC thermogram (Fig. 3), the solidification started with undercooling. As it can be seen from SEM micrographs and DSC curve, this alloy solidified in three consecutive steps during cooling the liquid. First the AgZr phase (marked as 1, Fig. 2 a) with faceted growth morphologies began to solidify at 1098 K. During the second solidification step that overlapped the peak of the first solidification a binary eutectic of AgZr and $(CuAg)_{10}Zr_7$ (marked as 2) started to solidify. The remaining liquid is consumed until the final product (that is, the m-phase + AgZr + $(CuAg)_{10}Zr_7$) solidifies, which is a ternary eutectic (marked as 5). The peak temperature of solidification of the eutectic is 1082 K measured during cooling (Fig. 3). The m-phase solidified independently in some places due to local segregation. In those areas the m-phase is needle-like. A very small amount of $CuZr_2$ phase was observed in the sample, which indicates that the solidification did not take place under equilibrium conditions. The calorimetric signal of $CuZr_2$ formation is not observed in the DSC thermogram, because the volume of this phase is very small or this formation is overlapped with another process.

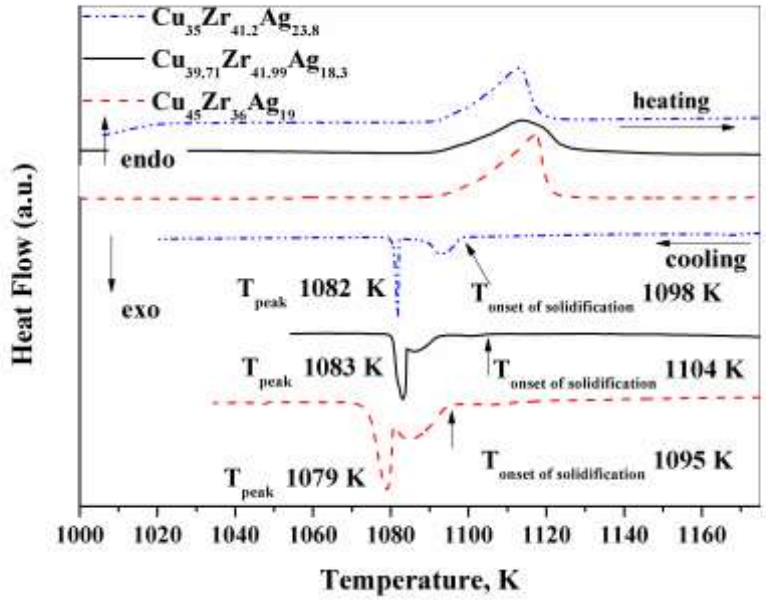

Fig. 3: DSC thermograms of heating and cooling at 5 K/min (0.083 K/s)

In the $Cu_{39.71}Zr_{41.99}Ag_{18.3}$ alloy, the solidified phases were the same as in the previous case indicating that also this composition does not correspond to the eutectic one, in contrast with the calculation by Kang et al. [8]. The solidification temperatures had almost the same values, while the structure had different appearance (Fig. 2d). The solidification started at 1104 K with the formation of the AgZr phase. The surface of primary solidified AgZr (Fig. 2d, marked as 1) needles was not flat, which implies that primary AgZr is covered by AgZr of the binary eutectic. A smaller volume fraction of primary AgZr crystals was observed in this sample than in the previous and following one. The m-phase could be detected only between the $(CuAg)_{10}Zr_7$ and AgZr crystals, which indicates that degeneration of ternary eutectic takes place. The AgZr phase of the ternary eutectic solidified on the primary solidified AgZr phase and the $(CuAg)_{10}Zr_7$ phase of the ternary eutectic solidified on the binary solidified $(CuAg)_{10}Zr_7$ phase. So the m-phase of the ternary eutectic is settled down between the AgZr needles and $(CuAg)_{10}Zr_7$.

The volume of m-phase here was the smallest compared to the three compositions proposed in literature as ternary eutectic compositions. In this sample a little volume of $CuZr_2$ phase was found as well (Fig. 2d, marked as 4).

Examination of the microstructure of ternary eutectic published by Kündig et al. [6] ($Cu_{45}Zr_{36}Ag_{19}$) has revealed that the solidification of this sample takes place in a different way (Fig. 2g) than in the previous samples. The DSC thermogram indicates three processes upon cooling (Fig. 3). An additional experiment was performed to identify the primary phase. The microstructure of the sample quenched at 1150 K can be seen in Fig. 4a. The m-phase solidifies primarily between 1114 K and 1083 K (Fig. 4b). The microstructure of the sample quenched at 1053 K features that the subsequent reaction is solidification of the ternary eutectic (Fig. 4c) of AgZr, $(CuAg)_{10}Zr_7$ and m-phases. The ternary eutectic solidification occurred in such a way that the m-phase of ternary eutectic solidified into the primary m-phase. The major volume of $CuZr_2$ phase was found in this sample. A solid transformation could be seen in the DSC thermogram at 1048 K. Taking into account the structure, this sample is located on another liquidus surface than the previous two compositions. Examined compositions are in the neighborhood of this composition but neither of them solidifies in one step according to DSC measurements.

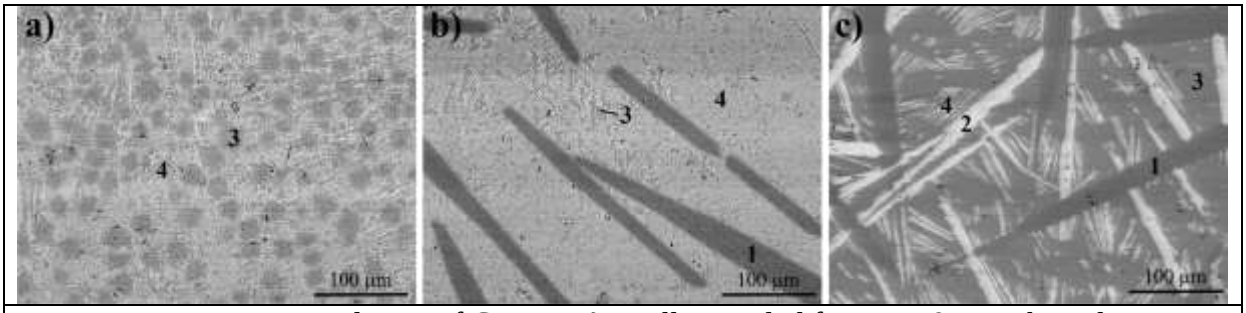

Fig. 4: Microstructure evolution of $Cu_{45}Zr_{36}Ag_{19}$ alloy cooled from 1150 K with cooling rate of 4 K/min (0.066 K/s) and quenched at 1150 K (a), 1083 K (b) and 1053 K (c) in water: 1 – m-phase, 2 – AgZr, 3 – $(CuAg)_{10}Zr_7$, 4 – eutectic structure

To determine the melting and ternary eutectic temperatures, thermal analysis of these three samples has been carried out. There is no standard definition in literature as on how to determine the liquidus temperature based on DSC measurements. Furthermore, there is no agreement whether the peak, endset or onset temperatures should be taken into consideration. Some researchers use the heating curve [29], some use the cooling curve [30], yet others use both [31]. It is usually difficult to analyze the liquidus temperature of metallic liquid especially in case of amorphizable alloys because of supercooling during the cooling process. In present work the liquidus temperatures are determined using the DSC heating curves according to [32-34]. The influence of heating rate on the endothermic curve of the DSC is also taken into account. The effect of heating rate on the onset temperature (T_{onset}), peak temperature of melting (T_{peak}) and final temperature of melting (T_{endset}) was revealed from the DSC profiles for the three above-mentioned compositions. The temperatures obtained from the intercepts on the y-axis for T_{onset}, T_{peak} and T_{end} are summarized in Table 2. The values of statistical correlation parameter are above 0.8. The difference in temperatures is below 1.5 K for T_{peak} and T_{end}. The liquidus temperatures for these samples are very close but the structures are different, so the three compositions do not belong to the same liquidus surface. The value of solidus temperature is found between 1090.9 K and 1095.5 K. On the contrary, the solidification behavior of ternary eutectic can be revealed much better with the cooling scans, because the melting process is overlapped with other melting processes. Thus, the ternary eutectic solidifies at an average temperature of 1081 ± 2 K, which is close to the value published by Kündig (1088 K) and He (1074.8 K).

3.3 Microstructure of master alloys

The primary solidified phases in master alloys are shown in Fig. 5. It can be seen that the liquidus projection is very complicated. In the present projection only five areas of liquidus projection have been verified by analyzing the microstructure: area of liquidus miscibility gap, primary Ag-solid solution, AgZr, m-phase and $(CuAg)_{10}Zr_7$.

The area of primary Ag-solid solution goes down to the composition with 20 at% Ag content as predicted by He et.al. [7] and there is no separate area of Ag-solid solution in the center of ternary diagram as predicted Kang et al. [8]. This area is bounded to the right by the surface of primary AgZr and to the left by the liquid miscibility gap which is practically in the center of the ternary diagram. Dendrites of Ag-based solid solution demonstrated in Fig. 6 contained 9-20 at% of Cu and 2-8 at% of Zr, respectively, measured by EDX. In the samples, which composition was close to the boundary between the liquid + primary Ag-solid solution and liquid + primary AgZr, two phases solidified as primary phases from the liquid (Fig. 5). It cannot occur under equilibrium conditions excluding the solidification of an alloy with eutectic composition. Note that cooling a master alloy in arc-melting equipment does not provide equilibrium conditions.

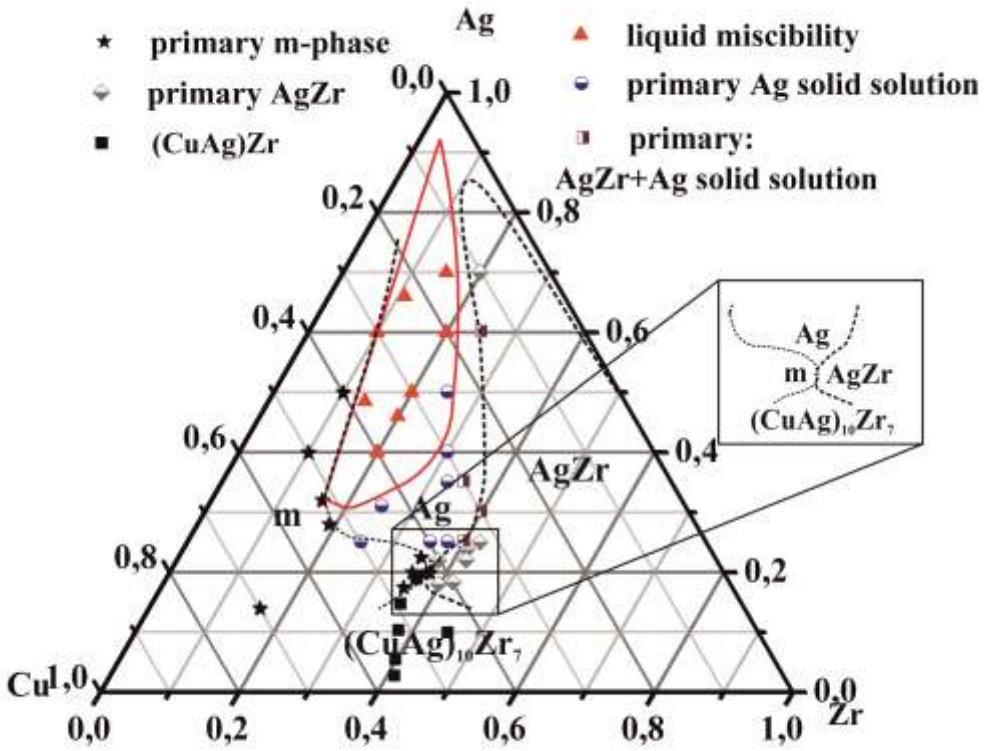

Fig. 5: The primary solidified phases and liquid separation observed in master alloy (cooling rate ~100 K/s). Dotted lines represent the liquidus troughs based on the harmonization of experimental results and the calculated phase diagrams.

The sample $Cu_{35}Zr_{40}Ag_{25}$ is a unique example of this fact (Fig. 6). SEM images demonstrate faceted AgZr crystals (marked as 1) solidified primarily and simultaneously with the dendrites of Ag-solid solution (marked as 2) but these phases do not solidify as a eutectic. Primary AgZr phases were observed in several cases with Ag content varying from 18 at% to 70 at%, as was predicted by Kang et al. [8]. The AgZr phase contains 10-16 at% of Cu, the $(CuAg)_{10}Zr_7$ phase 6-8 at% of Ag, respectively, as in the DSC samples. The primary solidified phases in the master alloy (Fig. 5) were similar to the primary solidified phases formed after the DSC cycles, where a controlled cooling rate was applied. Different primary phases were identified if the compositions of the samples were near the eutectic valley. For example, in the case of $Cu_{45}Zr_{36}Ag_{19}$ alloy the $(CuAg)_{10}Zr_7$ was the primary phase in the master alloy (Fig. 2h), while m-phase was the primary phase in the sample with controlled cooling (Fig. 2g) suggesting that the m-phase was deeper undercooled than $(CuAg)_{10}Zr_7$.

Apart from the primary phases the samples contain more or less volume of eutectic structure. In the master alloys the eutectic structure was much finer than in the DSC samples (Figs. 2). Also the composition of the eutectic is shifted. For instance, in the case of $Cu_{39.71}Zr_{41.99}Ag_{18.3}$ alloy the composition of eutectic was 51 at% Cu, 28 at% Zr and 21 at% Ag in the DSC sample and 40 at% Cu, 31 at% Zr and 29 at% Ag in the master alloy based on SEM observations. Namely, the Ag content increased and Cu content decreased, the Zr content did not change. In $Cu_{45}Zr_{36}Ag_{19}$ and $Cu_{35}Zr_{41.2}Ag_{23.8}$ master alloys the composition of eutectic structure was the same as in the abovementioned alloy.

Projection based on the microstructure of the master alloys related to the non-equilibrium state. However, there are fields of this liquidus projection, which are identical to the two published liquidus projections related to the equilibrium state.

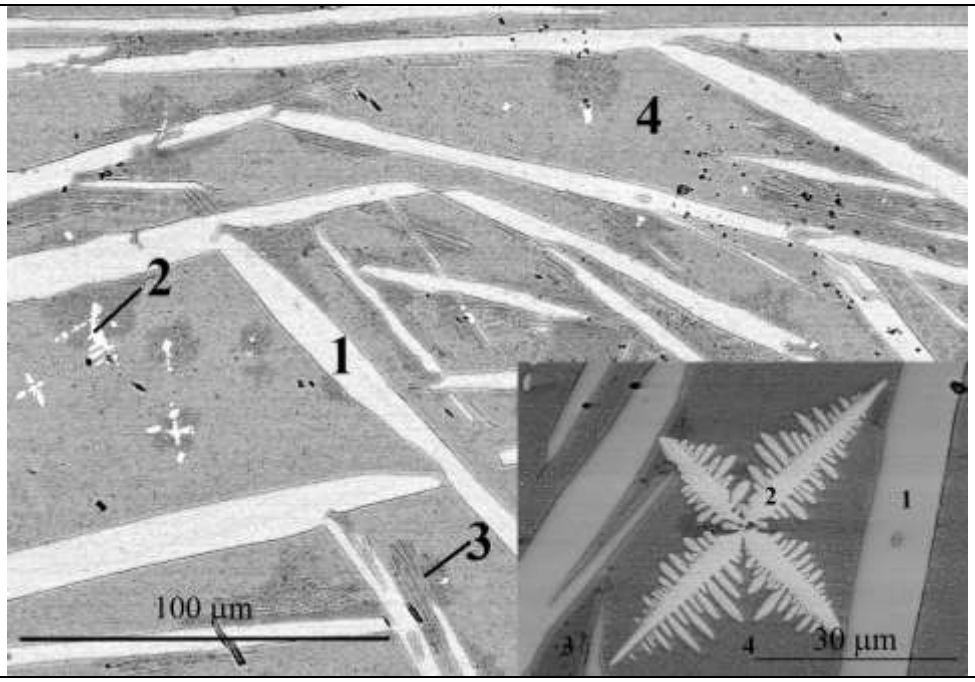

Fig. 6: SEM micrographs of the $Cu_{35}Zr_{40}Ag_{25}$ master alloy (a) and a higher magnification image with Ag-dendrite (b): 1 – AgZr, 2 – Ag-solid solution, 3 – m-phase and 4 – eutectic structure

3.4 Microstructure of wedge-shaped samples

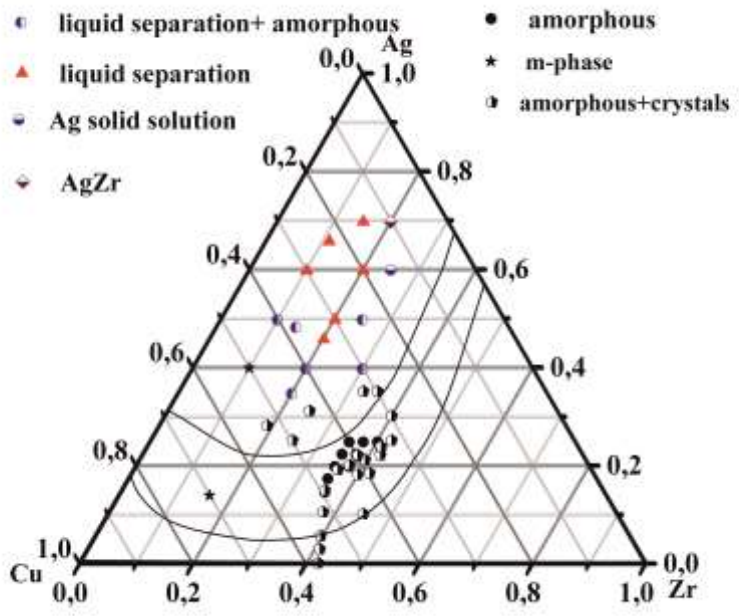

Fig. 7: The primary solidified phases, liquid separation and amorphous phase observed in wedge-shaped samples at the thickness of 0.5 mm where the cooling rate was ~7000 K/s. Two lines represent metastable miscibility gap and spinodal compositions, respectively predicted by Kang et al. [8]

Owing to the rapid cooling rate the microstructures were different from the previous ones: in some cases amorphous or amorphous/crystalline structure formed, and fully crystalline structure formed in some samples as well.

Considering the wedge-shaped samples of the same compositions, amorphous structure was observed in the region near the tip up to a maximum wedge thickness of 2 mm. The bases of the wedges were fully crystalline in all samples. Literature data reported 6 mm fully amorphous sample for this system [17] but inclusion of oxygen leads to a decrease of the maximum thickness of amorphous part. The formed structures of wedge-shaped samples at a thickness of 0.5 mm are presented in Fig. 7. This thickness was chosen in order to deal with bulk amorphous sample and not with ribbon. The cooling rate here was about 7×10^3 K/s [25]. The spinodal and metastable liquid miscibility gap curves published by Kang et al. [8] were added to the experimental diagram. It features that the fully amorphous area (marked as black circles) is narrower than the calculated one and is located between the spinodal and metastable liquid miscibility gap curves. Fully amorphous structure with a thickness above 0.5 mm was divided into two areas: the first area featured those compositions where the primary solidified phase was the m-phase in the master alloy (Fig. 5 and 7). The second area belonged to the compositions situated near the boundary between Ag-solid solution and AgZr phase liquidus surfaces, where two phases solidified as primary phase but did not form a eutectic structure. The results demonstrate that the m-phase shows the lowest driving force of nucleation in this system. The AgZr and Ag-solid solution have been formed also from an undercooled liquid but they have higher driving force of nucleation, therefore, fully amorphous structure has not been obtained.

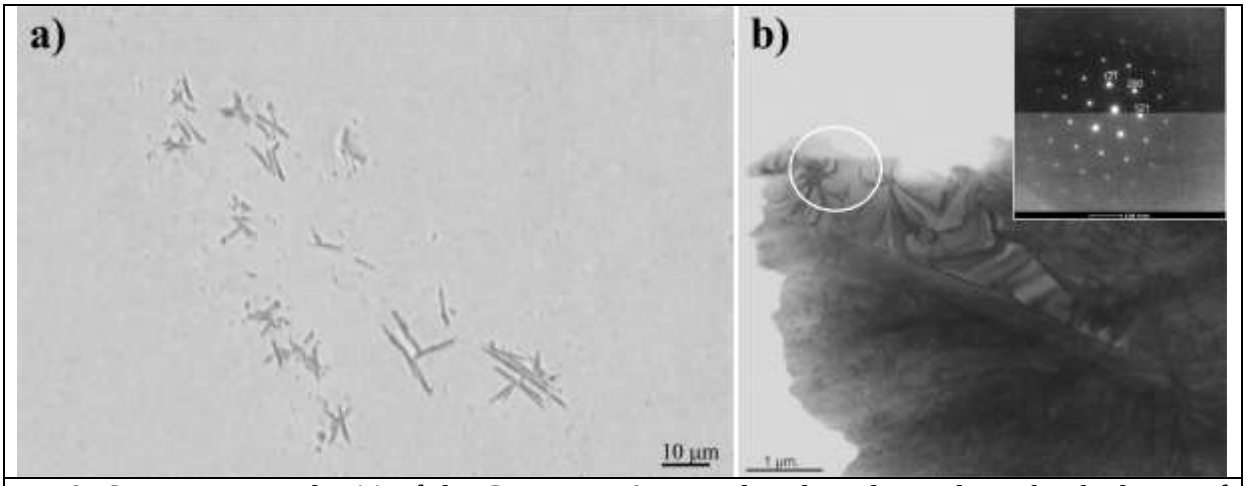

Fig.8**:** SEM micrographs (a) of the $Cu_{42.5}Zr_{37.5}Ag_{20}$ wedge-shaped sample at the thickness of 0.5 mm showing needle-like crystals and TEM bright field image of the needle-like crystals (b). The diffraction pattern (right upper corner) obtained from the area marked by white circle.

The $Cu_{42.5}Zr_{37.5}Ag_{20}$ is situated in the amorphizable area, and this alloy becomes amorphous owing to high cooling rate in the copper mould. In this case the primary solidified phase is m-phase both at a cooling rate of 5 K/min and in the master alloy. Based on SEM observations, the first appeared crystals in amorphous matrix are generally needle-like bent crystals (Fig. 8 a). Further TEM measurements are presented in Fig. 8 b. Bright field TEM image of the crystal showed stripes caused by diffraction contrast, which demonstrated how much the crystal was bent. According to ED patterns the needle-like crystals were not single crystals. Some parts of the crystal showed to be monoclinic, other parts were tetragonal. Slight differences could be observed between the monoclinic and tetragonal unit cells:

monoclinic unit cell with $\boldsymbol{a}_0$=0.480 nm, $\boldsymbol{b}_0$=0.740 nm, $\boldsymbol{c}_0$=0.480 nm, β=91.5±0.8°; tetragonal unit cell with $\boldsymbol{a}_0$=0.472 nm, $\boldsymbol{c}_0$=0.730 nm. This may be caused by chemical differences or ordering-disordering of the constituting elements. Besides, in some ED patterns the reflections had a diffuse character. The measured average composition of two needle-like crystals was: $Cu_{20}Zr_{50}Ag_{30}$.

The amorphous/crystalline composite could be obtained due to liquid separation with a silver content up to 50 at% [27]. The ternary liquid decomposed into one Ag-rich liquid (L_1) and another liquid being rich in Cu and Zr (L_2), and the latter forms the amorphous phase. The boundaries of the liquid ternary miscibility gap have been enlarged owing to high cooling rate [27].

In $Cu_{35}Zr_{41.2}Ag_{23.8}$ alloy the structure (Fig. 2c) was very different from the slowly cooled structure. In the matrix needle-like phases appeared: one had an elevated Ag-content with low Zr-content ($Cu_{25}Zr_{13}Ag_{62}$) and the other had elevated Cu-Zr content ($Cu_{43}Zr_{31}Ag_{26}$). A 50 μm thick layer developed on the surface of the wedge which was an amorphous/crystalline composite. Typical eutectic structure was not visible in the wedge. In $Cu_{39.71}Zr_{41.99}Ag_{18.3}$ alloy a needle-like phase solidified in the matrix (Fig. 2f), which composition was the same as that of the abovementioned Cu-Zr rich phase ($Cu_{43}Zr_{31}Ag_{26}$). Eutectic structure was not visible either in this case.

In $Cu_{45}Zr_{36}Ag_{19}$ alloy the primary phase was not the m-phase (Fig. 2i) in contrast to the most slowly cooled sample. The volume of eutectic structure obviously augmented with respect to the master alloy or DSC sample (Fig. 2i). The composition of eutectic structure was $Cu_{39.5}Zr_{38.1}Ag_{22.4}$.

4. Conclusions

The bulk glass forming alloy system can be strongly supercooled; therefore amorphous sample can be obtained. It is difficult to study solidification in such systems due to this phenomenon. The investigation of the Cu-Zr-Ag ternary system led to the following results:

1. It has been demonstrated experimentally that the proposed ternary eutectic compositions ($Cu_{45}Zr_{36}Ag_{19}$ [6], $Cu_{39.7}1Zr_{41.99}Ag_{18.3}$ [8] and $Cu_{35}Zr_{41.2}Ag_{23.8}$ [7]) published in literature are not true eutectics according to DSC and SEM measurements. The eutectic composition published by Kündig et al. [6] ($Cu_{45}Zr_{36}Ag_{19}$) was the closest to the ternary eutectic composition based on its microstructure. The liquidus temperatures of the above mentioned compositions were as follows: 1112.5 K, 1108.9 K and 1111.3 K, respectively, and the primary phases were: AgZr and, in the latter case, the m-phase.
2. The primary phases upon solidification were identified in all the alloys cooled at three different rates: 0.083 K/s (controlled cooling in the DSC), about 100 K/s (master alloys cooled in the arc furnace) and about 7000 K/s (samples cast in a wedge-shaped mould).
3. Based on the primary solidified phases liquidus projection of the Cu-Zr-Ag system has been covered. The central part of the liquidus projection of the ternary Cu-Zr-Ag system is determined based on the experimental results and the phase diagrams of the two ternary calculated systems. These data particularly confirm the two liquidus projections published in literature up to date. It has been shown that the field of liquid-liquid separation exists and the field of primary Ag-solid solution is not a separate area (opposite to Kang's theory). The liquidus projection in the Cu-Zr-Ag system has been successfully defined.

4. It has been shown that the m-phase has lower tendency to formation and growth with respect to the $(CuAg)_{10}Zr_7$ phase in this system.
5. The amorphization ability is influenced by the type and number of the primary solidified phases. In the wedge-shaped samples fully amorphous structure at the thickness of the wedge greater than 0.5 mm has been developed only in those compositions where the primary solidified phase was the m-phase or two phases solidified together as primary one.
6. It has been shown that the possibility of amorphization is very closely related to the phases formed during solidification of undercooled liquid. The experimental data confirmed that the fully amorphous area is narrower than the calculated one and is located between the spinodal and metastable liquid miscibility gap curves [8].

References

[1] X. Xiong, Y. Liu, G.J. Zhou, Y. Luo, T.L. Li, X.S. Li A. Inoue, W. Zhang, T. Zhang, K. Kurosaka, J. Alloys Compd. 563 (2013) 55-62
[2] Weibing Liao, Yangyong Zhao, Jianping He, Yong Zhang, J. Alloys Compd. 555 (2013) 357-361
[3] W. Zhou, X. Lin, J.F. Li, J. Alloys Compd.552 (2013) 102-106
[4] A.A. Kündig, M. Ohnuma, T. Ohkubo, T. Abe, K. Hono, Scripta Mater. 55 (2006) 449-452
[5] X.C. He, H. Wang, H.S. Liu, Z.P. Jin, Comp. Coupl. Phase Diagr. Thermoch 30 (2006) 367-374
[6] D.H. Kang, I.H. Jung, Intermetallics 18 (2010) 815-833
[7] K. K. Song, P. Gargarella, S. Pauly, G. Z. Ma, U. Kühn, J. Eckert, J. Appl. Phys. 112 (2012) 063503
[8] K.K. Song, S. Pauly, Y. Zhang, B.A. Sun, J. He, G.Z. Ma, U. Kühn, J. Eckert, Mater. Sci. Eng. A 559 (2013) 711–718
[9] K.-H. Kang, I. Sa, J.-C. Lee, E. Fleury, B.-J. Lee, Scripta Mater. 61 (2009) 801–804
[10] J. Antonowicz, D.V. Louzguine-Luzgin, A.R. Yavari, K. Georgarakis, M. Stoicae, G. Vaughand, E. Matsubaraf, A. Inoue, J. Alloys Compd. 471 (2009) 70-73
[11] J. Dutkiewicz, L. Jaworska, W. Maziarz, T. Czeppe, M. Lejkowska, M. Kubıcek, M. Pastrnak, J. Alloys Compd. 434–435 (2007) 333-335
[12] F.Q. Meng, K. Tsuchiya, F.X. Yin, S. Ii, Y. Yokoyama, J. Alloys Compd. 522 (2012) 136– 140
[13] Z. Liu, R. Li, G. Liu, W. Su, H. Wang, Y. Li, M. Shi, Acta Mater 60 (2012) 3128–3139
[14] Y. Wu, H. Wang a, H.H. Wua, Z.Y. Zhang a, X.D. Hui a, G.L. Chen a, D. Ma, Acta Mater. 59 (2011) 2928–2936
[15] W. Zhang, F. Jia, Q. Zhang, A. Inoue, Mater. Sci. Eng. A 459 (2007) 330-336
[16] X. Ou, G.Q. Zhang, X. Xua, L.N. Wang, J.F. Liu, J.Z. Jiang, J. Alloys Compd. 441 (2007) 181-184
[17] G.F. Ma, H.F. Zhang, H. Li, Z.Q. Hu, J. Alloys Compd. 513 (2012) 273–276
[18] B. Subramanian, S. Yugeswaran, A. Kobayashi, M. Jayachandran, J. Alloys Compd. 572 (2013) 163-169
[19] L.K. Zhang, Z.H. Chen, D. Chen, X.Y. Zhao, Q. Zheng, J. Non-Cryst. Solids 370 (2013) 31–36
[20] H. Fredriksson, Y. Arai, T. Emi, M. Haddad-Sabsevar, H. Shibata, Mater. Trans. 39 (1998) 587-595
[21] Y.H. Zhou, H.Z. Zhao, K.H. Zhang, J. Less-Comm. Met. 138 (1988) 7-10
[22] X.C. He, Y.M. Wang, H.S. Liu, Z.P. Jin, J. Alloys Compd. 439 (2007) 176-180

[23] K. Tomolya, D. Janovszky, M. Sveda, N. Hegman, A. Roosz, Mater. Sci. Forum 649 (2010) 93-99
[24] D. Janovszky, K. Tomolya, A. Sycheva, G. Kaptay, J. Alloys Compd. 541 (2012) 353-358
[25] D. Janovszky, K. Tomolya, A. Sycheva, P. Pekker, A. Roósz, J. Alloys Compd. doi.org/10.1016/j.jallcom.2012.12.067
[26] A. Castellero, D.H. Kang, I.H. Jung, G. Angella, M. Vedani, M. Baricco, J. Alloys Compd. 536 (2012) S148-S153
[27] H. Nishikawa, Y. Hamada, T. Tekemoto, J. Electronic Materials 38-12 (2009) 2610-2616
[28] M.A. Parvez, M. Medraj, E. Essadiqi, A. Muntasar, G. Denes, J. Alloys Compd. 402 (2005) 170–185
[29] J. Lapsa, B. Onderka, C. Schmetterer, H. Ipserb, Y. Yuan, G. Borzone, Thermochim. Acta 519 (2011) 55–58
[30] D. Minic, D. Manasijevic, V. Cosovic, N. Talijan, Z. Zivkovic, D. Zivkovic, M. Premovic, J. Alloys Compd. 517 (2012) 31–39
[31] D.S. Petrovic, G. Klancnik, M. Pirnat, J. Medved, J. Therm. Anal. Calorim. 105 (2011) 251–257
[32] A. Jamil, T. Kousksou, Y. Zeraouli, J.-P. Dumas, Thermochim. Acta 471 (2008) 1-6